Clim Dyn
DOI 10.1007/s00382-015-2669-z

Influence of small-scale North Atlantic sea surface temperature patterns on the marine boundary layer and free troposphere: a study using the atmospheric ARPEGE model

Marie Piazza[1] · **Laurent Terray**[1] · **Julien Boé**[1] · **Eric Maisonnave**[1] · **Emilia Sanchez-Gomez**[1]

Received: 31 July 2014 / Accepted: 18 May 2015

Abstract A high-resolution global atmospheric model is used to investigate the influence of the representation of small-scale North Atlantic sea surface temperature (SST) patterns on the atmosphere during boreal winter. Two ensembles of forced simulations are performed and compared. In the first ensemble (HRES), the full spatial resolution of the SST is maintained while small-scale features are smoothed out in the Gulf Stream region for the second ensemble (SMTH). The model shows a reasonable climatology in term of large-scale circulation and air–sea interaction coefficient when compared to reanalyses and satellite observations, respectively. The impact of small-scale SST patterns as depicted by differences between HRES and SMTH shows a strong meso-scale local mean response in terms of surface heat fluxes, convective precipitation, and to a lesser extent cloudiness. The main mechanism behind these statistical differences is that of a simple hydrostatic pressure adjustment related to increased SST and marine atmospheric boundary layer temperature gradient along the North Atlantic SST front. The model response to small-scale SST patterns also includes remote large-scale effects: upper tropospheric winds show a decrease downstream of the eddy-driven jet maxima over the central North Atlantic, while the subtropical jet exhibits a significant northward shift in particular over the eastern Mediterranean region. Significant changes are simulated in regard to the North Atlantic storm track, such as a southward shift of the storm density off the coast of North America towards the maximum SST gradient. A storm density decrease is also depicted over Greenland and the Nordic seas while a significant increase is seen over the northern part of the Mediterranean basin. Changes in Rossby wave breaking frequencies and weather regimes spatial patterns are shown to be associated to the jets and storm track changes.

Keywords Air–sea interaction · The Gulf Stream · North Atlantic weather regimes · Storm track · Rossby wave breaking

✉ Marie Piazza
piazza@cerfacs.fr

[1] Sciences de l'Univers au CERFACS, SUC URA1875, CERFACS/CNRS, Toulouse, France

1 Introduction

Mechanisms of mid-latitude air–sea interaction have been studied since several decades for their potential impact on large-scale climate [see Kushnir et al. (2002) for a review]. As supported by many observational and modeling studies, the current view is that mid-to-high latitude climate variability is mainly reflecting the passive response of the ocean to atmospheric forcing on time scales ranging from weeks to decades. However, recent satellite observations and high resolution atmospheric and coupled simulations have suggested that the potential strength of the oceanic forcing might have been underestimated in the previous generation of climate models (Maloney and Chelton 2006; Chelton and Xie 2010). A strong and positive correlation between SST and surface winds at oceanic meso-scale suggests that the small-scale spatial variations of SST can drive surface winds that generate vertical motions through convergence and divergence at the surface. There is now compelling evidence that sharp sea surface temperature (SST) fronts substantially influence the marine atmospheric boundary layer (MABL) and the free troposphere (e.g., Minobe et al. 2008; Nakamura and Yamane 2009; Bryan et al. 2010). Recent studies have focused on the influence of SST gradients in regions of western boundary currents on the atmospheric boundary layer and the free troposphere. Using a high resolution atmospheric general circulation model forced by observations, Kuwano-Yoshida et al. (2010) have shown that the SST front associated to the Gulf Stream anchors a convective rain band due low level convergence and enhanced evaporation over the warmer flank, indicating significant vertical motion in the free troposphere. Perlin et al. (2014) have tested and demonstrated the sensitivity to small-scale air–sea interaction to the atmospheric model boundary layer mixing scheme. Two mechanisms are involved in the local atmospheric response to SST fronts: (1) changes in MABL stability (Wallace et al. 1989), with an increase of stability over cold water leading to higher vertical shear and lower surface wind speed through weakened momentum vertical transfer from the top of the MABL to the surface (on the opposite, a decrease of stability over warm water leads to lower vertical shear and higher surface wind speed through enhanced momentum vertical transfer); and (2) an hydrostatic pressure adjustment to surface air temperature (SAT) pattern due to the SST front. While the first mechanism has been suggested to have little impact on the vertically averaged wind (O'Neill et al. 2010), the second mechanism is related to the Lindzen and Nigam (1987) mechanism that ties SST fronts to anomalies of the surface pressure gradient (Feliks et al. 2004, 2007). The resulting vertical velocity at the top of the MABL has two components: (1) a thermal one that results from pressure-driven flow generated by hydrostatic pressure adjustment to the temperature of the MABL, and (2) a mechanical one that results from the Ekman pumping in the MABL due to large-scale atmospheric eddies. While the thermal component dominates the long-term means, the two components have similar contributions at weekly time scale at mid-latitudes (Brachet et al. 2012). Both responses contribute to set up a large-scale environment favorable to a recurrent development of storms and thereby to anchor the storm-track along the SST front. The thermal component of the response, called "oceanic baroclinic adjustment" by Nakamura et al. (2008), generates a low-level baroclinicity through the SAT gradient, that can then interact with the upper-level jet-stream. Recent studies further reveal that the location and strength of the upper-level jet stream strongly depend on the position and intensity of the SST gradient and this effect is increased when moist processes are included (Laîné et al. 2011). Finally, Putrasahan et al. (2013) have used regional coupled and forced atmospheric models to quantify the sensitivity of the above mechanisms to the considered spatial scales of oceanic fronts. Their experiments have shown that while the two mechanisms coexist at all scales, their relative influence may significantly vary, suggesting the importance of a good representing of both into high-resolution climate models. The interested reader can read the review by Small et al. (2008) for an extensive presentation and discussion of these ideas.

Previous modeling studies have mainly used very idealized SST front patterns or perpetual winter conditions to study the atmospheric response (Brachet et al. 2012). Other authors have performed case studies dedicated to specific storm events and use more or less idealized SST surface forcing perturbations (Giordani and Caniaux 2001; Booth et al. 2012). Recent papers have also searched for an influence on the storm-tracks. In the Pacific Ocean, Taguchi et al. (2009) have shown that the storm track activity over the Kuroshio Extension positively feedbacks onto the low-level baroclinicity via strong cross-frontal contrasts in sensible heat flux, as previously suggested by idealized studies (Nakamura et al. 2008; Brayshaw et al. 2008). They have suggested that this feedback contributes to maintain the storm track activity in the frontal region despite the monsoonal influence that acts to weaken the surface air temperature gradient in winter. Recently, the effect of the atmospheric response to the Gulf Stream on the wintertime storm track has been investigated by Small et al. (2014) with a high-resolution global atmospheric circulation model, using Eulerian diagnostics to determine the storm track response. Their results have shown that the SST front has a strong influence on the transient eddy heat and moisture fluxes as well as on the eddy meridional wind variance, the last effect being mainly confined to the boundary layer. Their results also are consistent with the shift of the location of the maxima of storm track towards the frontal location found by Woollings et al. (2010). In their discussion, Small et al. (2014) emphasize the importance of conducting experiments with different models to compare results that may be strongly model dependent, as also suggested by Perlin et al. (2014).

In this study, the main objective is to assess whether the mean local and remote atmospheric response to a realistic SST frontal zone (such as the Gulf Stream) is sensitive to its small-scale spatial features. We also investigate the storm-track response using lagrangian diagnostics. A key question is whether the storm track shows any sensitivity to oceanic front and associated SST gradients. Previous studies have suggested that realistic simulation of small-scale SST patterns influence upon the atmosphere can be properly simulated only if the mesh size of the atmospheric model is on the order of 50 km or below (Feliks et al. 2004; Minobe et al. 2008). However, Bryan et al. (2010) have suggested that improving the small-scale ocean–atmosphere coupling depends more on the atmospheric boundary layer mixing parametrization than on an increase of the atmospheric resolution beyond this threshold. Here we explore the mean atmospheric response sensitivity to a range of large-scale atmospheric circulation and SST conditions within a realistic setting using a global atmospheric model. A set of sensitivity experiments is performed with a high-resolution atmospheric general circulation model (AGCM) forced by spatially high-resolution daily observed SSTs. Two different types of SST boundary conditions are used to force the AGCM with the objective of improving the understanding of how small-scale SST patterns influence the MABL and the free troposphere as well as the large-scale atmospheric circulation. The first type is simply the raw global SST data set at daily frequency and high spatial resolution, while the second one is obtained by spatially filtering out the small-scale SST features over a rectangular area surrounding the Gulf Stream (SSTs are unchanged outside this box). Ensemble AMIP-type AGCM simulations are then performed with the two SST datasets. Potential differences between the two suggest the influence of small-scale SST patterns in the Gulf Stream region. We first study the influence of the latter upon the surface atmospheric response in terms of surface fluxes and MABL characteristics. We then study potential changes of the storm-tracks. Indeed Hoskins and Valdes (1990) have shown that the strong SST gradient across the Gulf Stream is collocated with low-level baroclinicity in the troposphere that anchors the storm track along the SST front. We also analyze differences between weather regimes properties and transitions to see whether it is possible to relate them to potential SST influence and storm-track response sensitivity to large-scale atmospheric background. We finally assess upper tropospheric wind and related Rossby wave breaking changes between the two experiments.

The paper is organized as follows: Sect. 2 describes the model configuration and experiments as well as the analysis metrics and observed datasets. Section 3 gives a brief evaluation of the atmospheric model mean climate. Section 4 reports results on the impact of small-scale SST on the marine boundary layer and surface fluxes. Section 5 focuses on the impact on the free troposphere, storm-tracks and surface cyclones characteristics and large-scale circulation over North Atlantic and Europe. Section 6 contains the discussion and a short summary as well as future work directions.

2 Methods

2.1 Atmospheric model configuration

We use a high-resolution version of ARPEGE-Climat general circulation model that is the atmospheric component of the CNRM-CM5 coupled model developed by the CNRM-CERFACS group (Voldoire et al. 2013). ARPEGE-Climat is derived from ARPEGE-IFS (Integrated Forecast System) numerical weather prediction model developed conjointly by Météo-France and European Center for Medium-Range Weather Forecast (ECMWF). It is a spectral model that relies on the hydrostatic and thin-layer approximations, with 31 vertical pressure levels on a reduced Gaussian grid (Hortal and Simmons 1991). The high resolution version operates with a T359 truncature which corresponds to roughly ~50 km horizontal resolution at mid-latitudes. The deep convection follows the scheme developed by Bougeault (1985) and occurs under both convergence of humidity at low layers and unstable vertical temperature profile conditions. The convection adjusts the unstable profile to a cloudy profile, which is assumed to be moist adiabatic. Surface flux parameterization is derived from Louis (1979). Note that all atmospheric data used for graphic purpose are interpolated to a regular latitude/longitude grid.

2.2 Observations and reanalysis data sets

The National Oceanic and Atmospheric Administration Optimal Interpolation (NOAA-OI data provided by NOAA/OAR/ESRL, http://www.esrl.noaa.gov/psd/; Reynolds et al. 2007) daily-mean interpolated SST and ice fraction are used as oceanic forcings for the global domain on a regular grid at 0.25° × 0.25° resolution. The time period covered extends from 1st September 2002 to 31st July 2011.

The ability of the model to capture the small-scale oceanic forcing has been evaluated through the comparison with observations. Observed sea winds from the advanced NASA QuickSCAT satellite scatterometer enabled to detect the fine structure of the atmospheric response to the small-scale SST gradients (Dunbar et al. 2006). Wind speed at 10 m height data set extends from June 1999 to November 2009 with a wind vector resolution of 25 km.

Dynamical biases and variability of ARPEGE-Climat are evaluated against the ECMWF latest global atmospheric analysis ERA-Interim (hereafter ERAI; Dee et al. 2011). The latter operates on a 0.75° × 0.75° regular grid and 60 pressure levels, and covers a time period ranging from 1st January 1979 to 31st December 2013.

2.3 Sensitivity experiment design

In order to study the sensitivity of the atmosphere to the representation of sharp SST fronts along the Gulf Stream/North Atlantic drift pathway, we perform two sets of atmospheric simulations forced by observed SSTs. For both sets, four members are performed with slightly different atmospheric initial conditions. The first one uses global high resolution NOAA-OI daily SST and sea-ice fraction from 1st January 2003 to 31 July 2011 (HRES experiment). The second experiment (named SMTH), uses the same SST as HRES with SSTs being spatially smoothed to a coarser horizontal resolution within a box defined by a rectangular domain over the Gulf Stream region from 30°N to 50°N

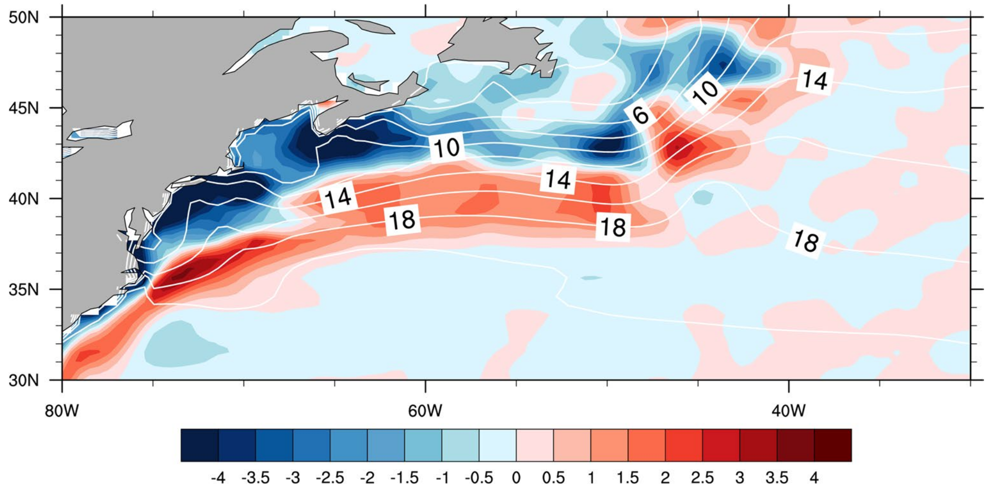

Fig. 1 Winter (DJF) SSTs in the Gulf Stream region: SST difference (in K) between HRES and SMTH experiments (*colors*) and SMTH climatology overlaid (*white contours* with a 2 K interval)

and from 30°W to 80°W (Fig. 1). This experimental design is made to detect the effect of realistic small-scale SST spatial variability associated with the Gulf Stream. In the SMTH experiment, the smoothing is only applied in the Gulf Stream domain rather than globally to avoid potential sources of variability associated with other regions of small-scale SST spatial variability that could interact with the signal associated with the region of interest. The identical SST forcing outside of the Gulf Stream region guarantees that remote influences are the same in both experiments. The smoothing has been performed using a conservative interpolation of NOAA-OI SST to a 4° × 4° rectangular grid and then linearly re-interpolated onto the original grid. Note that this method does not strictly conserve the SST, however the spatial average over the domain is close in both experiments (−0.25 K in average with a standard deviation of 0.07 K for the HRES-SMTH difference during extended winter over the considered period). In a narrow band of 2.5° along this domain boundaries, the SST resolution increases linearly to the NOAA-OI original resolution. Outside this domain, observed SSTs are identical in HRES and SMTH. The averaged SST pattern difference shows that spatial small-scale SST features strongly enhance the SST front with values up to 5–6 K in the western Atlantic and about 3–4 K in the central part of the front.

2.4 Surface heat fluxes decomposition

As we are interested in analyzing differences in the MABL response to SSTs between HRES and SMTH, we first want to compare the surface turbulent heat fluxes. The latter consist of two physical components, the fluxes of sensible heat Q_H and latent heat Q_E. Latent heat flux is calculated using a bulk formula,

$$Q_E = L \cdot \rho_a \cdot C_E \cdot W \cdot \left[q_s(T) - q_a\right] = L \cdot \rho_a \cdot C_E \cdot W \cdot Q \tag{1}$$

where L is the latent heat of vaporization, ρ_a the surface air density, C_E the transfer coefficient for the latent heat flux, W the surface wind speed, q_a the specific humidity of near surface air, q_s is the saturation specific humidity following the Clausius–Clapeyron equation calculated with T as the SST. The term $Q = q_s(T) - q_a$, the vertical difference of specific humidity near surface, is introduced for clarity. Similarly, sensible heat flux can be defined as:

$$Q_H = Cp \cdot \rho_a \cdot C_H \cdot W \cdot S \tag{2}$$

with Cp the specific heat capacity at constant pressure, C_H the transfer coefficient for sensible heat, and $S = T_a - T$ is a surface stability parameter, with T and T_a the SST and SAT at 2 m (in K), respectively. As the transfer coefficients were not archived during the simulations, C_E and C_H values are simply estimated from Eqs. (1) and (2) by a standard linear regression using daily values of Q_H, Q_E, W, Q and S at every grid point of the Gulf Stream domain (as defined on Sect. 2.3), and for both experiments separately. Now heat flux differences between the two experiments can be written as $\Delta Q_H = Q_{H\,HRES} - Q_{H\,SMTH}$ and similarly for Q_E. We define SMTH as the reference experiment and HRES as the perturbed one, thus the perturbed value of a variable X can be written $X_{SMTH} + \Delta X$. Assuming constant values for the air density, latent heat of vaporization, and specific heat capacity, one can then write changes in Q_E and Q_H as:

$$\begin{aligned}\Delta Q_E = L \cdot \rho_a \cdot (&\Delta C_E \cdot W_{SMTH} \cdot Q_{SMTH} + C_{E\,HRES} \\ &\cdot(W_{SMTH} \cdot \Delta Q + Q_{SMTH} \cdot \Delta W + \Delta Q \cdot \Delta W)) + \varepsilon_E\end{aligned} \tag{3}$$

and

$$\begin{aligned}\Delta Q_H = Cp \cdot \rho_a \cdot (&\Delta C_H \cdot W_{SMTH} \cdot S_{SMTH} + C_{H\,HRES} \\ &\cdot(W_{SMTH} \cdot \Delta S + S_{SMTH} \cdot \Delta W + \Delta S \cdot \Delta W)) + \varepsilon_H\end{aligned} \tag{4}$$

with the four components of ΔQ_H being the anomalous exchange coefficient, the anomalous stability, the anomalous wind speed and crossed term driven contributions (with a similar decomposition for ΔQ_E with anomalous specific humidity term instead of stability). ε_E and ε_H are residual terms from the use of regression lines to estimate the transfer coefficients.

2.5 Cyclone statistics tracking and Rossby wave breaking algorithms

The tracking algorithm of Ayrault and Joly (2000) is used to get cyclone statistics. It is based on the detection and tracking of relative vorticity (RV) maxima at 850 hPa with a 6-hourly time step. A recent description of the algorithm is provided by Michel et al. (2012). In the present study, we only retain systems whose RV is greater or equal to $2 \times 10^{-4}\ \mathrm{s}^{-1}$ to avoid the detection of relatively weak systems. A criterion on duration is also applied to retain storms lasting at least 2 days and remove all the detected but non-persistent ones. Their frequency of occurrence is of the order of 3–4 per week over the North Atlantic in the model. Grid-point tracks densities are spatially averaged with a halo of 200 km radius using a Gaussian weighting function.

The Rossby wave-breaking (RWB) detection method of Rivière (2009) is used to assess whether the presence of small-scale SST patterns could favor a specific type of RWB, either cyclonic or anticyclonic. The anticyclonic and cyclonic Rossby wave breaking could, in turn, trigger and maintain the positive and negative phase of the North Atlantic Oscillation depending on the latitude of the RWB changes (Strong and Magnusdottir 2008) or favor specific transitions between North Atlantic weather regimes (Michel and Rivière 2011). Rossby wave-breaking frequencies can be computed with the potential vorticity field on isentropic surfaces or with absolute vorticity field on isobaric surfaces. Michel and Rivière (2011) have checked that the two methods lead to qualitative similar results. Here the wave-breaking detection algorithm is applied to the absolute vorticity on pressure levels. More precisely, the method detects local inversions of the absolute vorticity gradient on a pressure level. To do that, all circumglobal contours of absolute vorticity ranging from -4.0×10^{-4} to $4.0 \times 10^{-4}\ \mathrm{s}^{-1}$ with an interval of $2.0 \times 10^{-5}\ \mathrm{s}^{-1}$ are detected and oriented from west to east. A wave-breaking region is defined as a local segment belonging to a circumglobal contour that is oriented from east to west. If the segment is mainly oriented along a northeast to southwest (southeast to northwest) direction, the wave breaking is of the anticyclonic (cyclonic) type. Note that as mentioned by Michel and Rivière (2011), it is necessary to estimate RWB on several vertical levels as the tropopause height varies with latitude, and RWB do not occur at the same level everywhere. Here we apply the algorithm to 4 vertical levels: 200, 250, 300 and 400 hPa and average the results.

3 Evaluation of the simulated climate

3.1 North Atlantic winter climate

We first evaluate the ability of the ARPEGE atmospheric model to produce a realistic North Atlantic climate mean state and its synoptic variability. Unless explicitly mentioned, we focus now on the extended wintertime period, from November to March (both included). As one of our objectives is to assess whether SST fronts can have an impact on large-scale circulation characteristics, we first investigate the ability of the ARPEGE model to represent the latter using a standard weather regime analysis.

3.1.1 Weather regimes

In order to evaluate the ability of ARPEGE to simulate realistically the prominent modes of low-frequency variability over the North Atlantic, we perform a classification in weather regimes for the extended winter (NDJFM hereinafter) period. Prior to the weather regime analysis, we have estimated the seasonal cycle of Z500 using the first two harmonics and subsequently removed it from the raw field to obtain daily anomalies. We first compare the HRES North Atlantic weather regimes with those obtained from ERAI. To determine the weather regimes, the daily geopotential height at 500 hPa pressure level (Z500 thereafter) is first used to perform an empirical orthogonal function (EOF) analysis in the North Atlantic domain (28.5°N–79.5°N, 79.5°W–28.5°E) from 1st January 2003 to 31st December 2010 (the optimal overlapping time period between HRES and ERAI). 25 EOFs (explaining more than 90 % of the total variance) are retained. Z500 is then partitioned into five clusters in the EOF phase space using the k-means algorithm, based on minimization of the total variance inside each cluster. First this methodology has been applied to ERAI and shows a classification into five weather regimes. Four of the five weather regimes of ERAI correspond to those initially described by Vautard (1990), namely the Scandinavian blocking (BL), the Greenland anticyclone (GA), the Atlantic ridge (AR) and the zonal regime (ZO). The fifth regime corresponds to the East Atlantic pattern (EAP); it shows a strong zonal extension thus can be seen as a variant of the ZO regime with a southward shift of the large depression from the north to the middle of the North Atlantic basin. Then the same methodology than the one used for ERAI has been applied to HRES. In HRES, the positive (GA regime) and negative (ZO regime) phases of the North Atlantic Oscillation are well represented (Fig. 2d, e, pattern correlations with ERAI ZO and GA are 0.95 and 0.97, respectively). A large anticyclonic structure centered on the North Atlantic with a zonal extent through the basin with a cyclonic structure

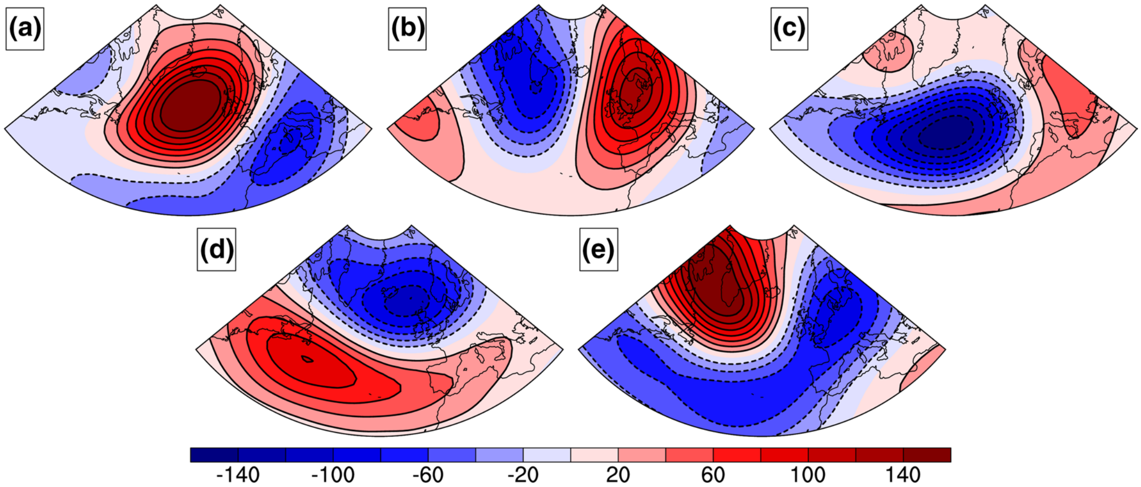

Fig. 2 HRES North Atlantic weather regimes in extended wintertime (November to March). Centroids of daily geopotential height at 500 hPa anomaly from climatology (in meters) over the period January 2003–December 2010 corresponding to the regimes **a** AR, **b** BL, **c** EAP, **d** ZO and **e** GA. From **a** to **e**, frequencies of occurrence are respectively 20.3, 19.0, 22.8, 23.2, 14.7 % (differences to ERA-Interim are 4.9, −5.0, 1.3, 1.0, −2.1 %, resp.)

over North and Western (Fig. 2a) can be related to AR with a pattern correlation with ERAI of 0.82. The fourth regime (Fig. 2b) shows a bipolar structure with a strong anticyclone over Northern Europe close to BL (pattern correlation is 0.81). The EAP regime exhibits a large zonal depression over the Atlantic basin, which extends up to Iceland and an anticyclone over Eastern Europe (Fig. 2c, pattern correlation with ERAI is 0.77). These results show that the spatial patterns of the simulated weather regimes are closely related to those of ERAI. Differences in frequencies of occurrence between HRES and ERAI are small for ZO, GA and EAP (1, −2 and 1 %, resp.) and slightly larger for AR (5 %) and BL (−5 %), but statistical significance may hardly be tested on such a short time period.

3.1.2 The jet stream at mid-latitudes

We now investigate the mean state and variability of the simulated eddy-driven jet over the North Atlantic. The 200-hPa zonal wind is defined as a proxy of the jet stream, as the simulated jet shows a maximum of intensity at 200 hPa pressure level, in agreement with ERAI. Figure 3a shows that the main path of the jet is accurately represented over North Atlantic in the model but with a very slightly reduced southwest-northeast tilt resulting in a slightly too zonal eddy-driven jet. Note also that the model has a very reasonable representation of the jet variability as depicted by the 200-hPa zonal wind standard deviation. The variability is particularly strong along the main path of the jet stream in the western Atlantic, south of Greenland and over the Mediterranean region (Fig. 3b). The high resolution ARPEGE model seems to have small upper tropospheric wind biases, while the current generation of lower resolution AGCMs are too zonal and generally underestimate latitudinal variability of the jet stream over North Atlantic during winter (Hannachi et al. 2013).

3.2 The frontal-scale air–sea interaction coefficient

Previous studies have estimated the observed and simulated air–sea coupling coefficient (or strength) to evaluate and quantify the surface wind response to SSTs over regions with strong ocean eddies and fronts (Maloney and Chelton 2006). Here the interaction is one-way only and there is no possible feedback from the atmosphere to the ocean as we use SST-forced AGCM simulations, so we use the term air–sea interaction coefficient instead. This coefficient quantifies the strength of the ocean forcing upon the atmosphere and is simply estimated by the regression coefficient between the spatial small-scale components of SST and near-surface wind speed in the HRES experiment (see Fig. 4e–h). We compare the simulated coefficient obtained by concatenating all four HRES members with the observed one derived from ocean 10-m height winds from QuickSCAT and NOAA-OI SST (Fig. 4a–d), for the optimal overlapping time period between HRES and QuickSCAT extending from January 2003 to November 2009. Here we consider both winter (DJF) and summer (JJA) to evaluate the sensitivity of the air–sea interaction strength to the seasonality in HRES compared to the observations.

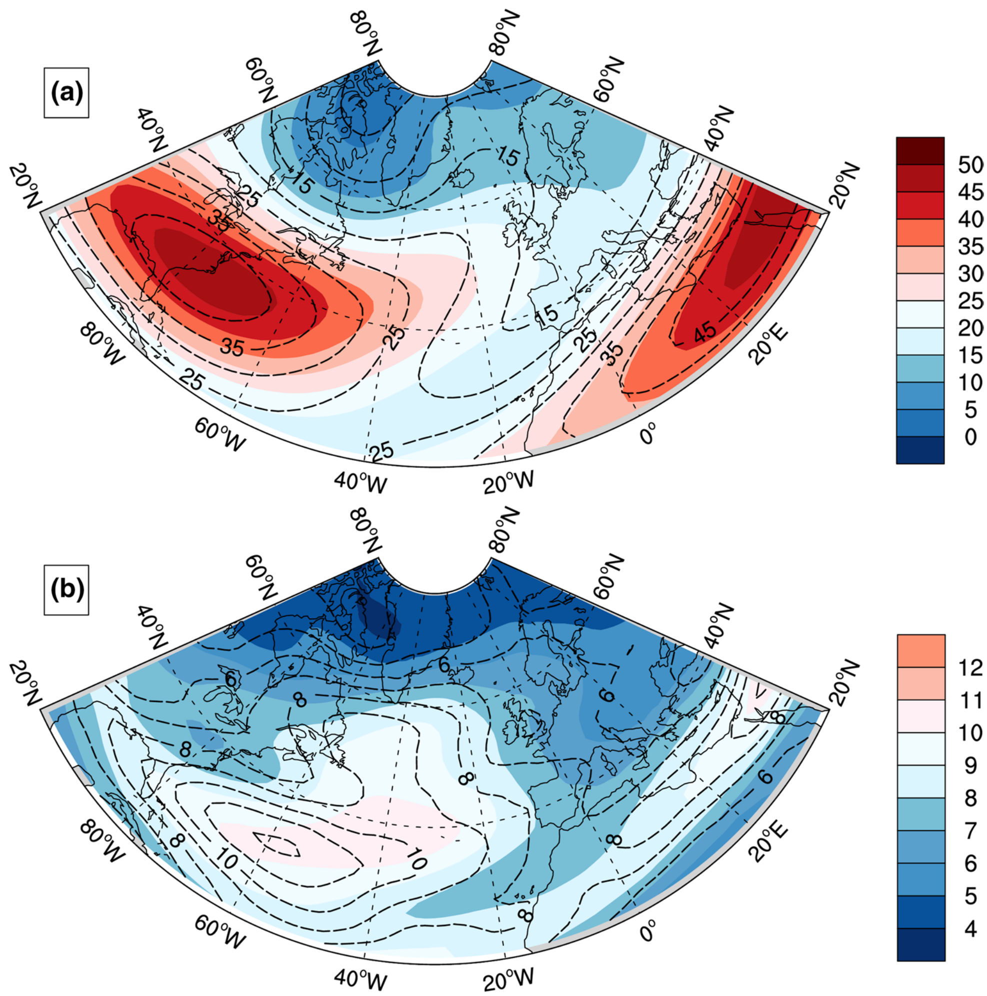

Fig. 3 Zonal wind at 200 hPa in extended wintertime (November to March) in the Gulf Stream region. **a** Mean and **b** standard deviation in HRES (*colors*, in m s^{-1}) and in ERA-Interim (*black contours*, with a contour interval of five and 1 m s^{-1} in **a** and **b**, respectively)

Small-scale spatial components of 10-m height wind-speed and SST have been derived from monthly field by subtraction of the large-scale component, the latter being obtained by spatial smoothing. Note that wind-speed is computed prior to the smoothing from daily values of zonal and meridional wind components. The smoothing is made for each sea point of the Gulf Stream domain (as defined in Sect. 2.3) by averaging all sea-point values within a circle of 300 km radius centered on the considered point. The small-scale oceanic forcing can reach values of about 6 °C, with negative and positive difference patterns possibly exceeding −3 and 3 °C respectively. Observations show small and coherent interacting structures all over the front. The model also exhibits oceanic forcing although the signal is smoother and amplitude of wind speed perturbations is slightly weaker than observed, especially in winter. For both observations and HRES, the correlation is larger in winter (0.75 and 0.67 in DJF, resp.) than in summer (0.72 and 0.33 in JJA, resp.). Small-scale oceanic forcing is more realistic in winter in the model (Fig. 4h) with a coefficient of interaction of 0.20 m s^{-1} K (0.29 in observations, Fig. 4d) compared to 0.11 m s^{-1} K in summer (Fig. 4g; 0.36 in observations, Fig. 4c). The ARPEGE model seems to have a reasonable representation of the small-scale air–sea interaction during winter. In summer, the poor representation of this interaction in the model suggests that the processes involved may be different in summer and in winter. This difference may be induced by the influence of the large-scale environment on the small-scale air–sea interaction. For instance, the enhanced stability of the atmospheric boundary layer in winter may explain the higher sensitivity of the atmosphere to the small-scale oceanic forcing compared to summer in the model. Due to the short time period considered here, it is difficult to assess whether the slight underestimation in winter of the simulated value is real or is due to sampling effect associated with the short observational dataset.

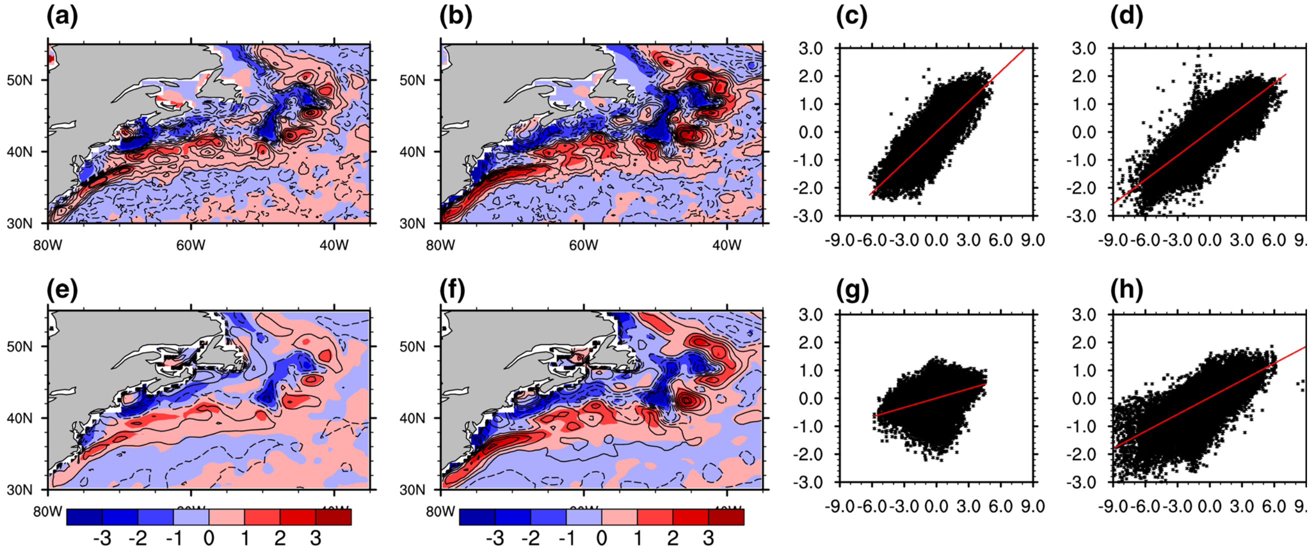

Fig. 4 **a**, **b**, **e**, **f** Maps of spatially high-pass filtered SST (*colors*) and wind speed at surface (contours, from −0.65 to 0.75 m s^{-1} with an interval of 0.15 m s^{-1}), mean in summer (JJA, **a**, **e**) and in winter (DJF, **b**, **f**), from 1st January 2003 to 31st July 2011. **a**, **b** Observations (AMSR-E and QuickSCAT); **e**, **f** HRES experiment. **c**, **d**, **g**, **h** Associated scatter-plots of space–time filtered SST (*horizontal axes*, in K) and wind-speed at surface (*vertical axes*, in m s^{-1}), in summer (JJA, **c**, **g**) and winter (DJF, **d**, **h**). **c**, **d** Observations (AMSR-E and QuickSCAT); **g**, **h** HRES experiment. The space–time filter consists in the same spatial high-pass filter as for maps (**a**, **b**, **e**, **f**) and on a 30-days running average. *Red lines* are regression lines (regression coefficients values are given in Sect. 3.2)

4 Local atmospheric response to small-scale SST patterns

4.1 Surface heat fluxes and MABL response

We first investigate the differences in turbulent heat fluxes between the two experiments described in Sect. 2.3 during extended winter (November to March). For the sake of clarity, we define SMTH as our reference experiment and anomalies as the difference between HRES minus SMTH. Both latent and sensible heat fluxes anomalies are strongly spatially related to SST anomaly with a pattern correlation of 0.82 and 0.81, respectively (Fig. 5). Anomalous turbulent heat fluxes are in average 30 % of the reference fluxes over warm water, with a maximum of 50 % (with values greater than 250 W m^{-2} anomaly) over the warmest SSTs. As noted by Brachet et al. (2012), there is a significant asymmetry between heat flux amplitude changes over warm and cold SST anomalies, in particular for the latent heat flux. Figure 5a, b, e, f shows that the decomposition using Eqs. (3) and (4) leads to an adequate reconstruction of the heat flux differences between HRES and SMTH. Analysis of the decomposition terms suggests that the contribution associated with the exchange coefficient C_E anomaly is by far, the dominant term for the reconstructed latent heat flux anomaly over the SST front (Fig. 5c). This coefficient depends both on wind speed and MABL stability, but the much smaller contribution to anomalous wind speed (Fig. 5d) suggests that the MABL stability is the main driver of the latent heat flux response to small-scale SST forcing. Others contributions of specific humidity parameter and cross-term anomalies are found to be negligible. Figure 5g shows that the near surface stability parameter S acts as the primary forcing of the sensible heat flux response to the small-scale SST anomaly. This result is in good agreement with Small et al. (2014). Note however that the sign of the contribution related to the cross-term of anomalous wind speed and near surface stability is opposite to the total sensible heat flux anomaly on the northeastern part of the Gulf Stream pathway (Fig. 5h). Others contributions of wind speed and transfer coefficient changes are found to be negligible.

We now investigate the dominant mechanism in the wind convergence ARPEGE response to the anomalous SST front. As mentioned in the introduction, two mechanisms are involved. The first mechanism is the hydrostatic adjustment due to pressure balance. If this mechanism is dominant, then the near-surface wind convergence is supposed to be related to the Laplacian of sea level pressure in terms of pattern and amplitude (Minobe et al. 2008; Takatama et al. 2012). The second mechanism is related to the downward momentum mixing mechanism, by which warmer SSTs destabilize the lower atmosphere and

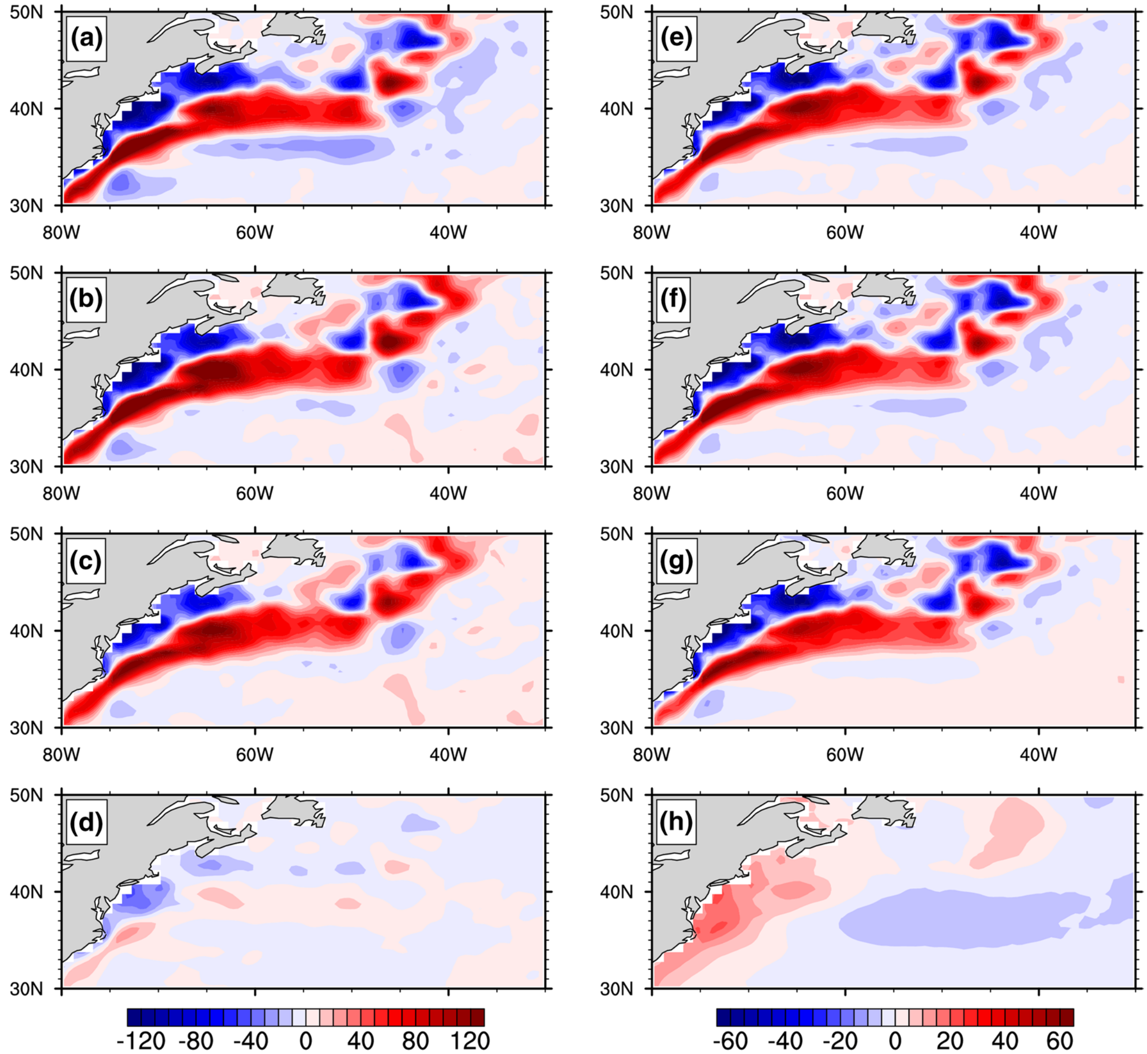

Fig. 5 **a**–**d** (**e**–**h**): Latent (sensible) heat flux difference (in W m^{-2}) between HRES minus SMTH, in extended winter (Nov–Mar). **a** (**e**) Latent (sensible) heat flux difference. **b** (**f**) As above but reconstructed using Eqs. (3) and (4). **c** (**g**) Main contribution to the total reconstructed latent (sensible) heat flux difference due to the transfer coefficient (surface stability parameter) difference. **d** (**h**) Second contribution to the total reconstructed latent (sensible) heat flux difference due to the surface wind speed (crossed term) difference

increase downward momentum transport from the top of the MABL to the surface, thus accelerating surface winds. If this mechanism is dominant, then near-surface wind divergence is proportional to the downwind SST gradient. As suggested by Small et al. (2008) and Kilpatrick et al. (2014), the respective contributions of the pressure adjustment and downward momentum mixing mechanisms depend on different factors such as the front length scale and the background flow intensity as well as the time-averaging performed. Here we perform an analysis of multi-year mean changes due to a large-scale SST front. As suggested by Takatama et al. (2012, 2015), it is important to separate the two contributions from these mechanisms in our model experiments. We first focus on the change of low-level wind convergence and assess which mechanism plays the dominant role if any. As shown in Takatama et al. (2012) the momentum convergence at surface (noted MCS, and expressed as horizontal convergence of near surface wind times ρ_a, with ρ_a the air density) can be expressed as the sum of contributions related to boundary layer pressure adjustment, the downward momentum mixing mechanism and the contribution of the horizontal advection. We use the first right hand side term of their Eq. (3) to get the contribution related to pressure adjustment, that is expressed as the Laplacian of the sea level pressure times $\varepsilon/(\varepsilon^2 + f^2)$, with f the Coriolis parameter and ε a linear damping coefficient. The constant value of 2.0×10^{-4} s^{-1} is used for ε, as suggested by Takatama et al. (2012). Figure 6 shows

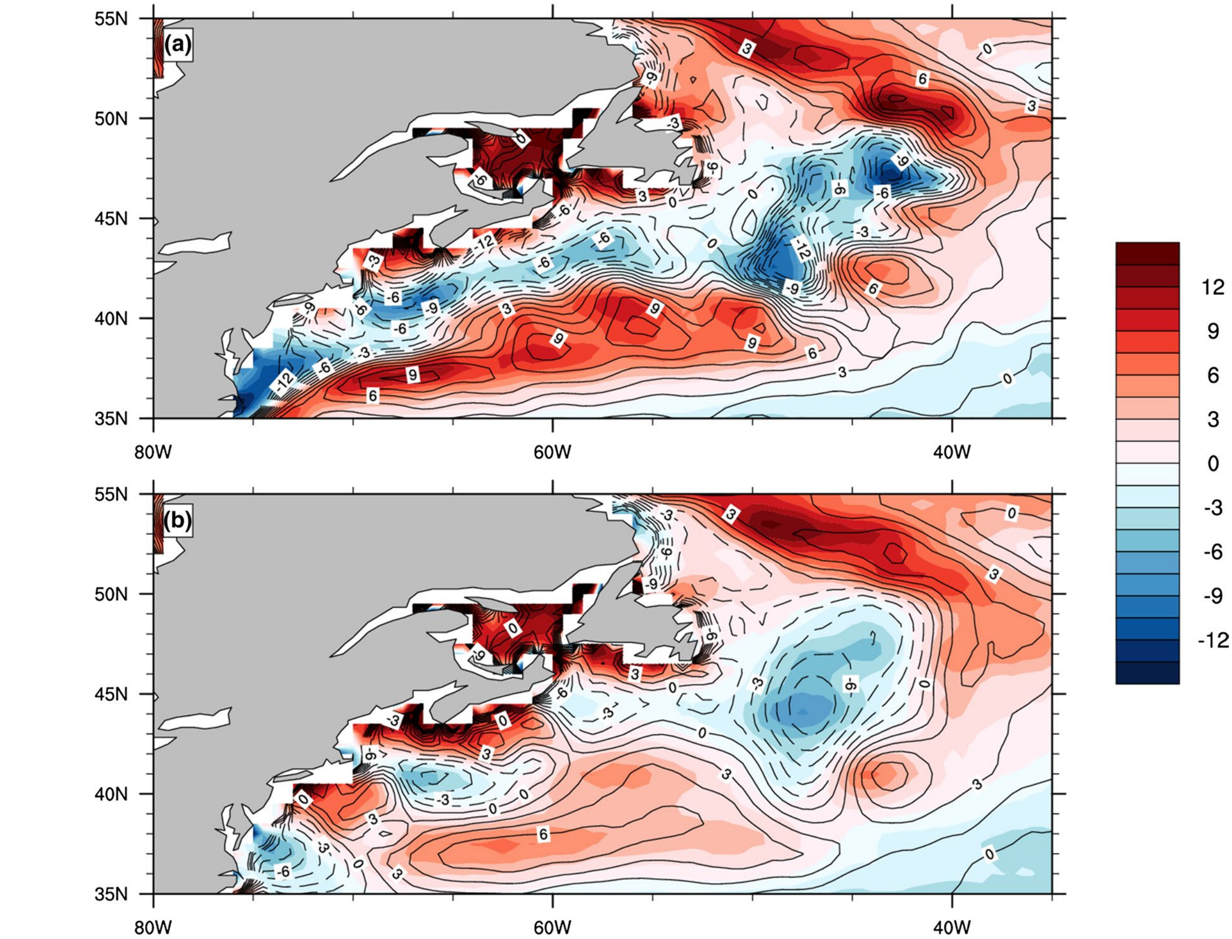

Fig. 6 Contribution of the boundary layer pressure adjustment term (color, 10^{-8} Pa m^{-2}) to the near-surface momentum convergence (contours, interval 1.5 × 10^{-8} Pa m^{-2}, negative values are *dashed*), see text Sect. 4.1 for details. **a** HRES, **b** SMTH. A slight spatial smoothing has been applied to all fields. Extended winter (Nov–Mar)

the degree of similarity between MCS and the pressure adjustment contribution. Note that the two terms are presented with the same units so they can be quantitatively compared. This relationship exists both in HRES and SMTH but with much better spatial agreement and coherence as well as larger amplitude in HRES, with low-level wind convergence along the warm side of the SST front while divergence prevails on the cold side. The zonal spatial coherence in HRES contrasts with the SMTH scattered aspect along the frontal zone. Note that the Laplacian of sea level pressure is closely tied to the Laplacian of the MABL temperature (taken here as the mass weighted temperature between the near surface and 850 hPa) rather than SST (pattern correlation of 0.79 vs. 0.38 in HRES, 0.7 and 0.33 in SMTH). The strong coherence between wind convergence and Laplacian of sea level pressure in HRES is in good agreement with observations, as shown in Shimada and Minobe (2011). In both experiments, the pattern and amplitude of the pressure adjustment term are very similar to that of the MCS, suggesting that the other contributions are rather small.

4.2 Tropospheric local response

To assess the deeper response in the free troposphere, we now investigate cloud and precipitation responses. Figure 7 shows cloudiness and convective precipitation anomalies over the SST front. Cloudiness anomalies (Fig. 7a) roughly follow the spatial pattern of the SST front with reduced and enhanced cloudiness over the cold and warm side of the front, respectively, in agreement with recent observations (Liu et al. 2014). This is clearer in the western part of the front (where the front has a west-east orientation) than in the eastern part (south-north orientation). The sign of cloudiness anomalies suggests that there is a negative short-wave

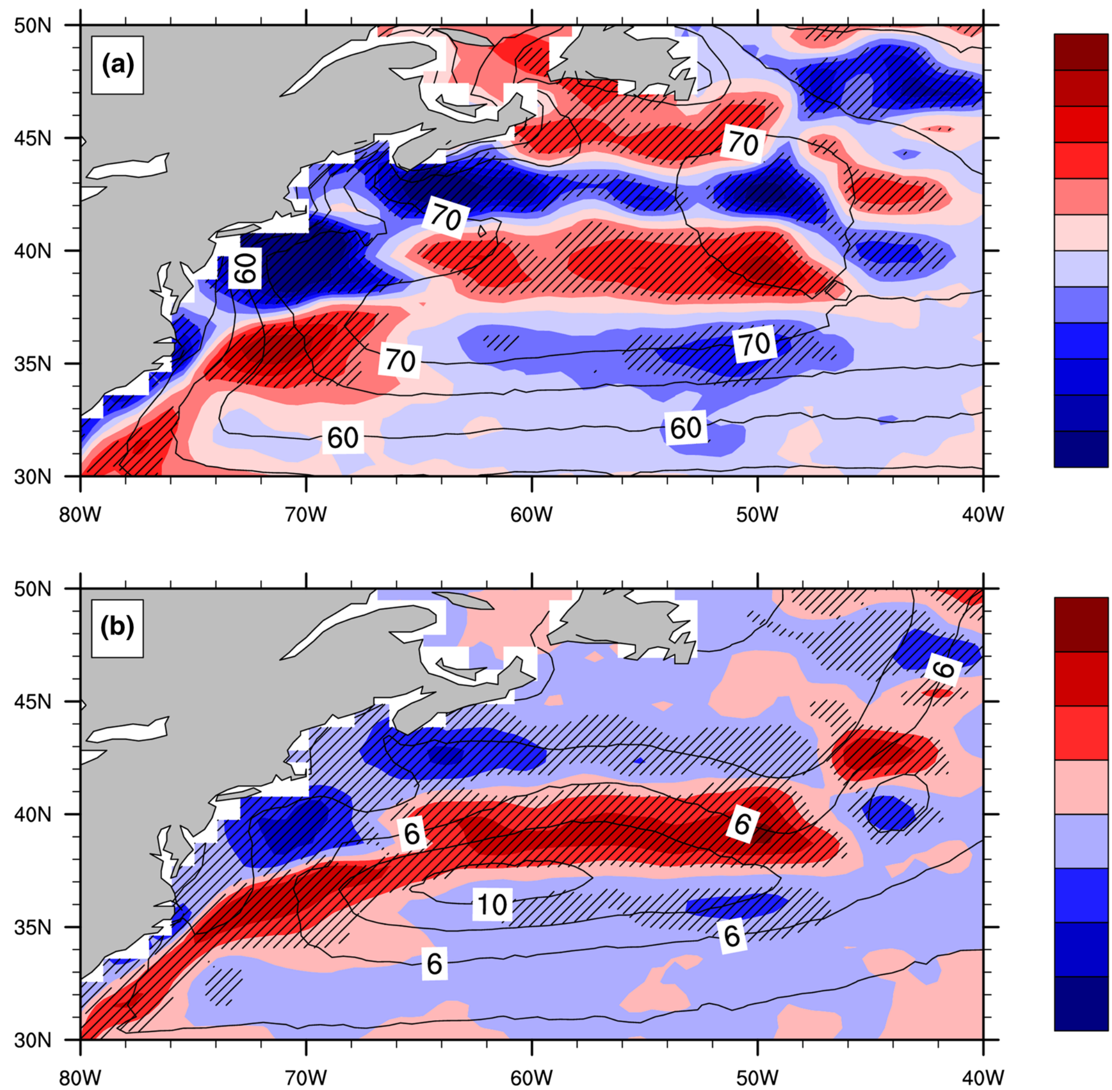

Fig. 7 Differences between HRES and SMTH of **a** cloud fraction (in %) and **b** convective precipitation (in mm day^{-1}), for extended winter (Nov–Mar). *Black contours* are SMTH values and hatching shows regions where the difference is *t*-statistically different from 0 at the 5 % significance level

radiative feedback of the atmosphere to the SST front as the cloudiness changes would possibly tend to reduce the SST front amplitude in a coupled framework. A strong convective precipitation anomaly (about one third of reference precipitation on average, and over 60 % over the warm water, Fig. 7b) indicates a deep local impact of the Gulf Stream SST front in the free troposphere, consistent with Kuwano-Yoshida et al. (2010). Indeed, positive anomalous precipitation over warm SST anomaly is consistent with turbulent heat fluxes anomalies, through the combination of the moisturizing of air by enhanced latent heat flux and SST-induced positive vertical motion over the warm flank of the front.

5 Remote atmospheric response to small-scale SST patterns

5.1 Upper tropospheric zonal wind response and Euro-Atlantic regimes

We first discuss whether small-scale SST patterns have any impact on the upper tropospheric zonal wind U_{ut}. Inspection of the U_{ut} difference between HRES and SMTH shows a clear large-scale response marked by displacements of the jets (Fig. 8). In HRES, U_{ut} shows an increase by 20 % south of Greenland and over the Irminger Sea, and a similar decrease over the central North Atlantic downstream of the maximum of the jet. The subtropical jet exhibits a

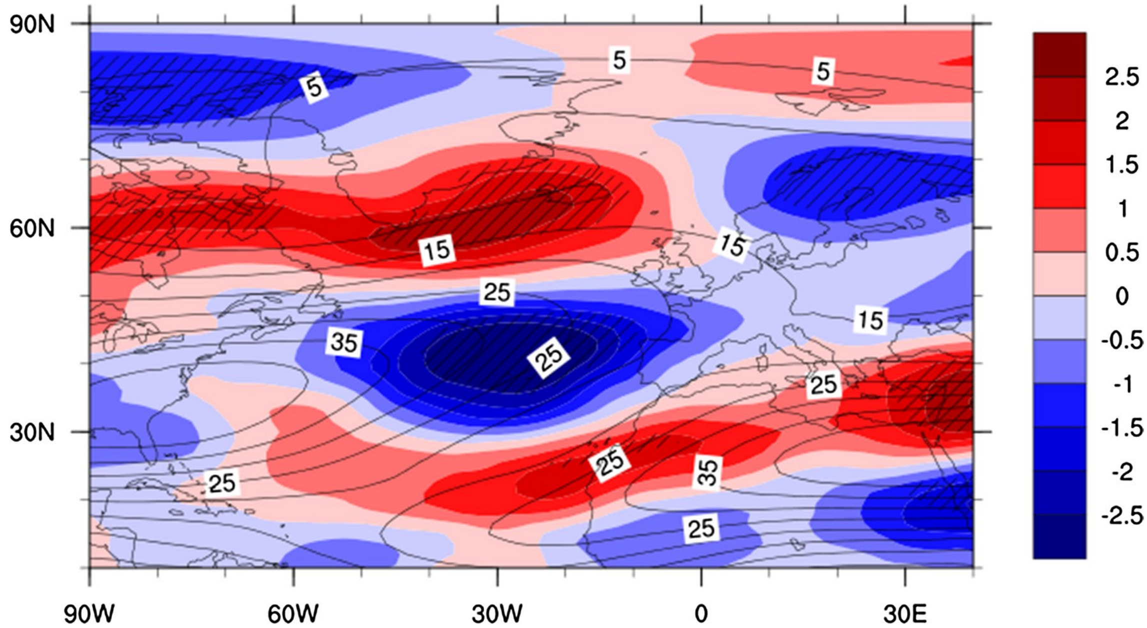

Fig. 8 Difference between HRES and SMTH of the mean zonal wind averaged between 200 and 300 hPa isobaric surfaces (in m s^{-1}), for extended winter (Nov–Mar). *Black contours* show the mean SMTH climatological values. Hatching shows regions where the HRES-SMTH difference is *t* statistically different from 0 at the 10 % significance level (note that statistical significance does not reach the 5 % level)

Table 1 Number of transitions between two persistent (minimum 5 days length) and directly consecutive weather regimes over North Atlantic, for HRES (italic) and SMTH (underline) experiments

From	AR		BL		EAP		ZO		GA	
To										
AR			***14***	**16**	*7*	2	*8*	8	*8*	3
BL	*7*	7			*6*	10	***12***	**13**	*1*	0
EAP	*6*	4	*2*	6			*8*	7	***23***	**30**
ZO	*8*	7	***16***	**13**	*5*	8			*2*	2
GA	***19***	**20**	*1*	0	*9*	8	*0*	3		

The bold values indicate the 5 predominant types of transitions, underlying that they are the same in both experiments. However the statistical significance has not been tested, given the relatively small number of events considered. Extended winter (Nov–Mar)

significant northward shift in particular over the eastern Mediterranean region. These large-scale changes can be linked to changes in RWB occurrence (see Sect. 5.3).

The low-frequency winter atmospheric variability of the North Atlantic-European region and its relationship with the small-scale SST patterns is investigated based on the comparison of weather regimes between HRES and SMTH. The cluster decomposition (described in Sect. 3.1.1) is applied to concatenated Z500 fields from both experiments. Then a composite analysis of the Z500 is performed between HRES and SMTH for the five weather regimes. Statistical significance is calculated with a non-parametric approach by bootstrapping. Note that only regimes with a persistence of at least 5 days are retained and that a transition is defined as the direct succession between two different weather regimes.

The weather regimes analysis reveals that some spatial patterns exhibit small but statistically significant differences between the two experiments. In particular, the EAP and ZO regimes have a slightly stronger eastward extension in HRES compared to SMTH. Differences in frequency of occurrence between HRES and SMTH weather regimes does not exceed ±1 % except for BL (2 %), and does not reveal significant changes. Preferred transitions remain the same between the two experiments (Table 1). The most favorable transition is GA towards EAP in both experiments, but is reduced by 25 % in HRES compared to SMTH.

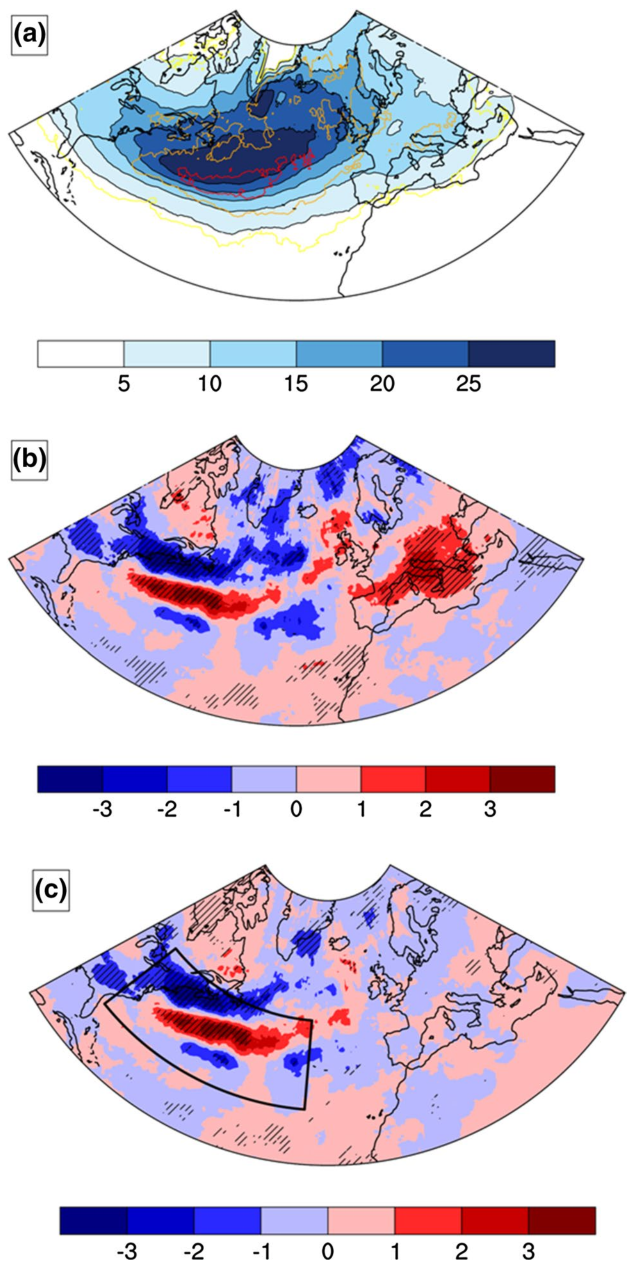

Fig. 9 Storm tracks density over North Atlantic during extended winter (Nov–Mar, in number of storm tracks per season). **a** HRES mean (colors and thin black contours) and standard deviation (*yellow* to *red* contours, from 2 to 6 with a stride of two storm tracks per season). **b** Composite of HRES compared to SMTH. Hatching shows regions where the difference is significantly different from 0 at the 5 % significance level. **c** Same as **b** but only for storm tracks that pass over the Gulf Stream region as represented by the *thick black contoured box*

5.2 Storm tracks

We now investigate the impact of the SST front in the Gulf Stream region on storm tracks over North Atlantic in winter. The horizontal resolution of ARPEGE has been shown to be fine enough to represent storms explicitly. A recent study from Michel et al. (2012) has shown a relationship between winter weather regimes over North Atlantic and storm tracks population and distribution. In the following, we refer as storm tracks the systems detected with the tracking algorithm (presented in Sect. 2.5) which last at least two consecutive days and reach a maximum of vorticity equal or superior to 2×10^{-4} s^{-1} for one time step at least. This filter removes all local minima of vorticity that may be detected but do not correspond to a realistic storm. Figure 9a shows the density of storm tracks per extended winter season over North Atlantic simulated in HRES. The Gulf Stream region and its eastward extension are the regions where the density is the largest, with more than 20 storm events per season in average. It is also the region with the largest interannual variability. Another storm track density maximum of similar amplitude occurs south of Greenland while a secondary one is located over the Mediterranean region. Previous studies have shown the impact of baroclinicity on storms generation and trajectories (e.g., Rivière 2009). Here we investigate whether the presence of small-scale SST patterns have any influence on the Atlantic storm tracks. The comparison between HRES and SMTH shows large and statistically significant differences in term of winter storm tracks density (Fig. 9b). Storm track density in HRES decreases over the northern part of the front and its eastward extension towards the Irminger Sea, as well as over the Nordic seas and Scandinavia, while it increases over the sub-tropical part of the front and the Mediterranean Sea. The former changes can be seen as a southward shift of the storm track density off the east coast of North America onto the maximum of SST gradient. This effect was already suggested by Woollings et al. (2010) but it has a stronger amplitude and wider geographical extent here as well as in Small et al. (2014). Using standard diagnostic such as band-pass filtered transient 850 hPa eddy heat fluxes and meridional wind variance to directly compare with results from Small et al. (2014), the ARPEGE model response seems to have a smaller amplitude (heat flux) or a different pattern (meridional wind). These differences may be partly related to the stronger SST smoothing used in Small et al. (2014) compared to ours (leading to larger changes in SST gradient amplitude in their study) and to different mean state biases.

The sensitivity of storm tracks response to small-scale SST in the Gulf Stream region to the large-scale atmospheric flow is further investigated by compositing storm tracks into the weather regimes in which they spent the most time (Fig. 10). First, the decomposition according to the weather regimes (Fig. 10a–e) shows that the storm track distribution over the Euro-North Atlantic domain depends

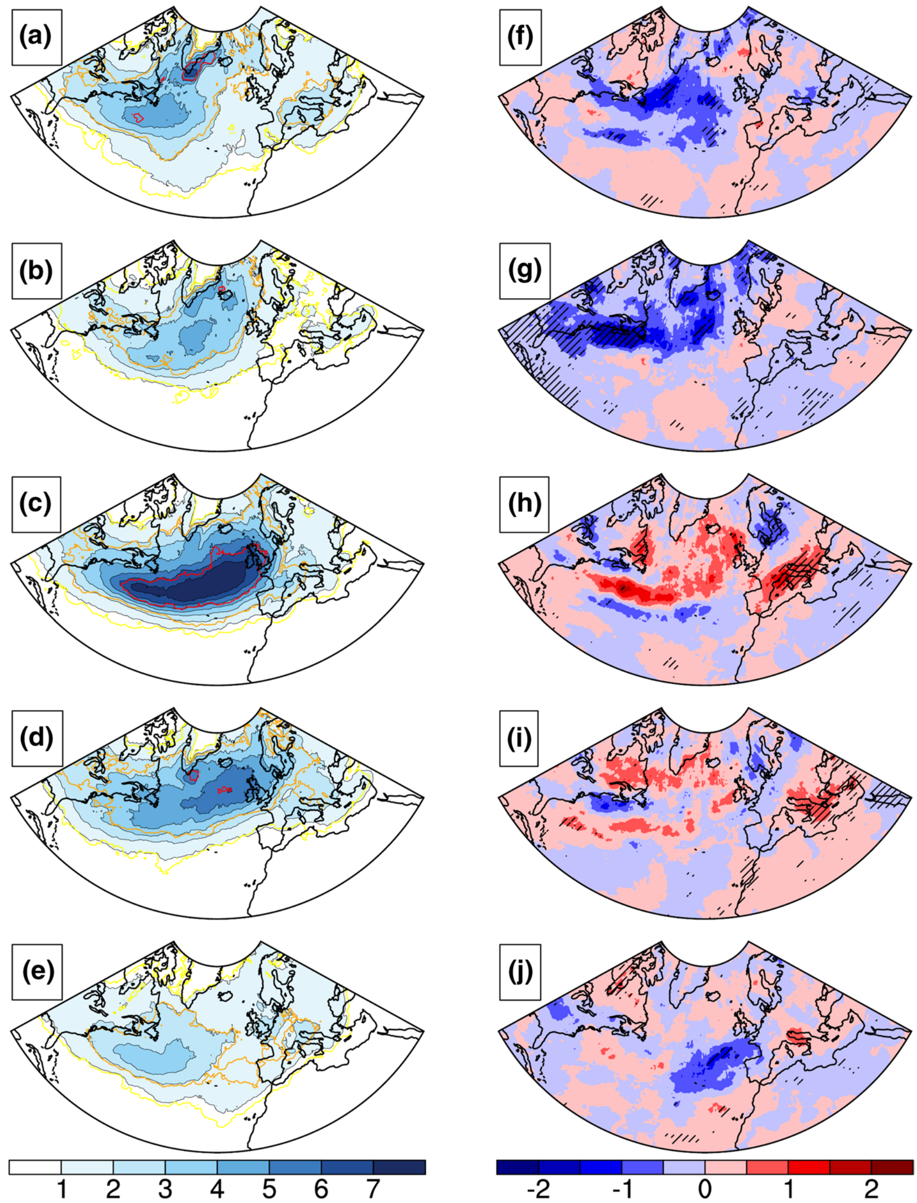

Fig. 10 Same as Fig. 9 but storm tracks are attributed to the five weather regimes of HRES and SMTH. **a**–**e** and **f**–**j** correspond respectively to AR, BL, EAP, ZO and GA. The standard deviation is given by *yellow*, *orange* and *red contours*, with values of 1, 2 and 4 storm tracks per season. Hatching shows regions where the difference is significantly different from 0 at the 5 % level

on the large-scale atmospheric flow. The EAP regime concentrates about 25 % of the total density over the main storm track with a spatial pattern very similar to the mean climatology. This model regime is a variant of the classical zonal regime although it has a slightly more zonal path in our model. It also presents a significant variability (more than four storm tracks per season over the central North Atlantic). Storm tracks over Mediterranean coastal area and Southern Europe are more or less evenly distributed among all weather regimes, except for BL. The large extension of the atmospheric blocking centered over the North Sea induces a northeastward deviation of the zonal mean flow over North Atlantic that prevents storm tracks from reaching Europe. Then the comparison between HRES and SMTH reveals that storm-track changes are specific to certain regimes (Fig. 10f–j). The BL and AR regimes experience a reduction of storms over the main storm-track axis and north of it. This reduction extends south and east of Greenland and to the Nordic seas, but the strongest effect occurs when the BL regime is excited. In contrast the EAP and ZO regimes show an increase in storm-track density slightly south of the SST front, and over the Mediterranean Sea. No significant change is detected for the GA regime. The spatial distribution of large-scale changes between HRES and SMTH shows intra-regime consistency that does not appear when considering all days together, and strong inter-regime contrasts. These results confirm the relevance of the storm attribution to weather regimes to study

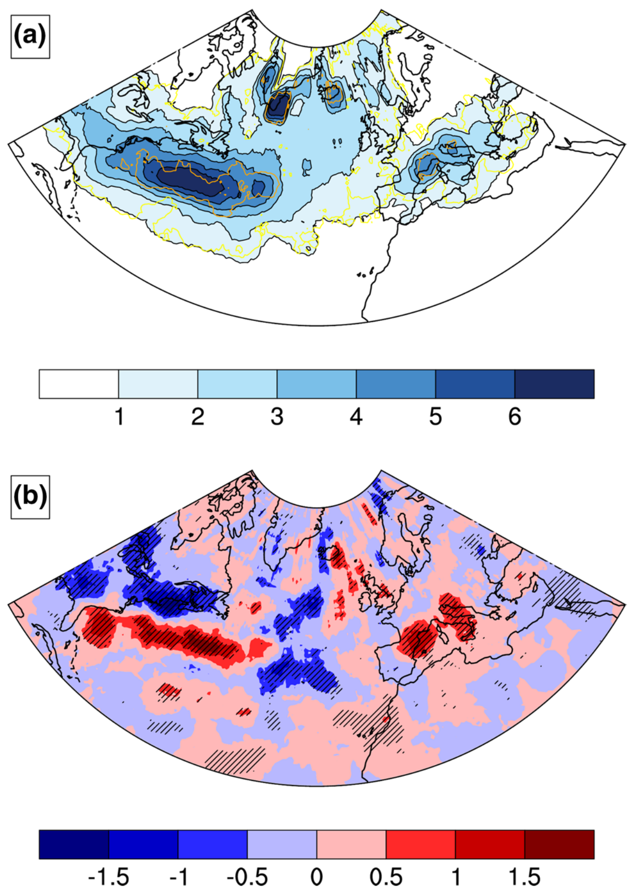

Fig. 11 Same as Fig. 9 but for density of storm generation

the storm-track response to small-scale SST forcing in the Gulf Stream region.

We ask now whether these changes reflect trajectory changes or storm generation changes. Figure 11 shows the difference in storm generation between HRES and SMTH. Over the North Atlantic and Europe domain, the spatial pattern of the difference between HRES and SMTH of the storm generation density (Fig. 11b) is close to that of Fig. 9b. The local response over the Gulf Stream front shows an increase of about 20 % of storm generation associated with spatial small-scale SST variability. Also, remote response of storm generation to the Gulf Stream SST front shows an increase of similar amplitude located at the north of the Mediterranean basin. These spatial pattern and amplitude of the differences between HRES and SMTH suggest that storm track density changes are primarily due to changes of storm generation spatial distribution in the Gulf Stream region and its northeastward extension as well as in the Mediterranean basin. The eastward orientation of the large-scale mean flow may explain the generally wider and eastward extension of the storm track density anomalies compared to the storm generation density anomalies in those regions. However, near the southeast part of Greenland and over the Barents Sea, storm generation changes cannot explain storm tracks density changes. Over those regions, Fig. 9b shows small and barely statistically significant decrease of storm track density. However these changes become significant when considering only the storm tracks that pass over the Gulf Stream region, hence that are directly impacted by the SST front. The direct impact of the small-scale SST on storm trajectories is isolated by filtering the storms that cross the Gulf Stream domain for at least one time step, here a 6-h period (Fig. 9c). Comparison between Fig. 9b, c shows that on the southeast of Greenland and over the Nordic Seas, the decrease of storm track density is due to storm trajectories changes. Two mechanisms can be involved in the local storm response above the SST front. First, enhanced surface heat fluxes above the warm side of the SST front in HRES compared to SMTH act to moisten and warm the air in the MABL that lead to an additional amount of latent heating that can fuel the storms passing above the warm side of the SST front. The opposite effect applies on the cold side of the front and explains the storm tracks density reduction near the coast. The second mechanism is related to baroclinicity changes due to the presence of enhanced SST and related air temperature gradients in the MABL. However, as the SST changes are typically of small spatial scale, it is not clear whether these baroclinicity changes can efficiently affect baroclinic waves (Woollings et al. 2010). The remote changes over the Mediterranean Sea are linked to the previously mentioned changes in EAP and ZO regime spatial patterns. As the EAP regime has the highest storm track density and is more zonal in HRES than in SMTH, the southwest-northeast tilt of cyclone pathways is reduced and more storms end up on the northern rim of the Mediterranean basin.

5.3 Links with Rossby wave breaking

We now investigate the role of RWB in association to the changes between HRES and SMTH. Figure 12 shows the winter climatology of RWB frequencies for SMTH averaged over four (200-, 250-, 300- and 400-hPa) isobaric surfaces. The Atlantic sector exhibits local maxima in the anticyclonic and cyclonic RWB. The most frequent anticyclonic RWB frequencies extend from the southwest Atlantic to the eastern Mediterranean with a maximum in the central subtropical Atlantic. The cyclonic RWB frequency map exhibits two maxima of smaller amplitude: the main one is located south of Greenland while a secondary one occurs slightly north of the Mediterranean region. These results are in good agreement with those of Strong and Magnusdottir (2008) using reanalysis data and a different RWB algorithm. It is useful at this point to summarize the effect of RWB on the zonal flow averaged over nearby longitudes. For anticyclonic RWB, the zonal flow is accelerated north of the latitude of breaking

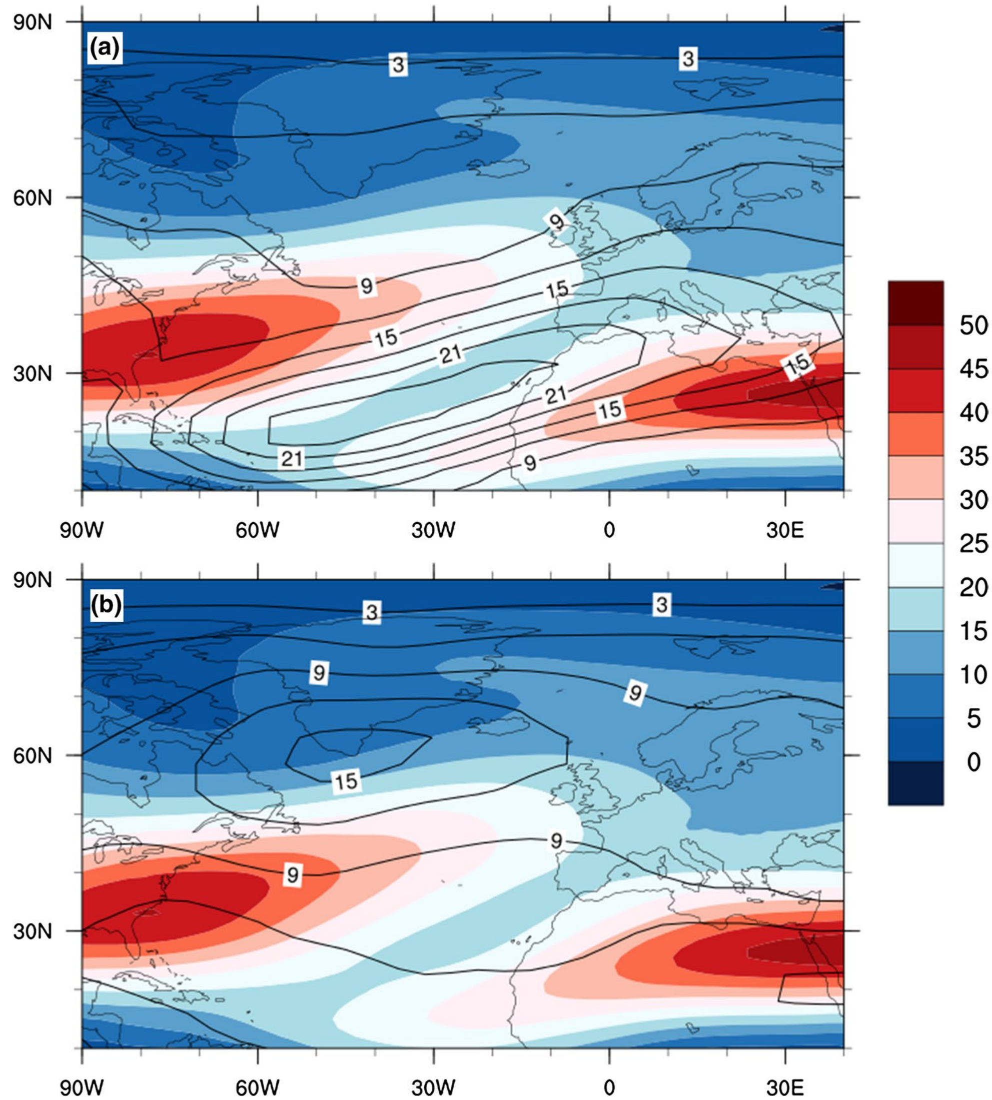

Fig. 12 **a** Anticyclonic and **b** cyclonic Rossby wave breaking frequencies (*thick black* contours, contour interval is 3×10^{-2} day^{-1}) averaged on 200-, 250-, 300- and 400-hPa isobaric surfaces, in SMTH experiment. These results are SMTH experiment in extended winter (Nov–Mar). *Shading* represents zonal wind averaged between 200 and 300 hPa (in m s^{-1})

and decelerated south of that latitude. For cyclonic RWB, the zonal flow is decelerated north of the latitude of breaking and accelerated south of that latitude. We now detail the RWB frequency differences between HRES and SMTH in relation with the upper-tropospheric zonal wind changes (Fig. 13). The main changes in anticyclonic RWB occur in the eastern Atlantic with an increase and decrease (20 and 10 %) off the coasts of Western Europe and Africa, respectively. The increase in the central and northeastern Atlantic would favor the accelerated zonal flow south of Greenland seen in Fig. 8. An increase (15 %) of cyclonic RWB occurs in the central Atlantic between 30N and 60N as well as over the northeast side of the Mediterranean region. The increase and northward displacement of the subtropical jet (see also Fig. 8 for its mean position in SMTH) is related to changes in both anticyclonic and cyclonic RWB over the subtropical Atlantic and northwestern Africa.

6 Summary

Two ensembles of simulations with the global high-resolution ARPEGE atmospheric model have been used to investigate the possible winter response of the atmosphere over the North Atlantic European domain to the presence of small-scale SST patterns. The two ensembles differ by the prescribed SST boundary forcing, that is spatially smoothed over the Gulf Stream region in one of the ensembles. It was first shown that the model has a realistic large-scale circulation climatology and reasonable representation of the winter small-scale air–sea interaction coefficient compared to the observations. Then the ARPEGE model has shown a strong local response to small-scale SST patterns in terms of latent and sensible heat fluxes, precipitation, and cloudiness. Amplitude of turbulent heat flux changes is about 30 % over the SST front, with a maximum of 50 %.

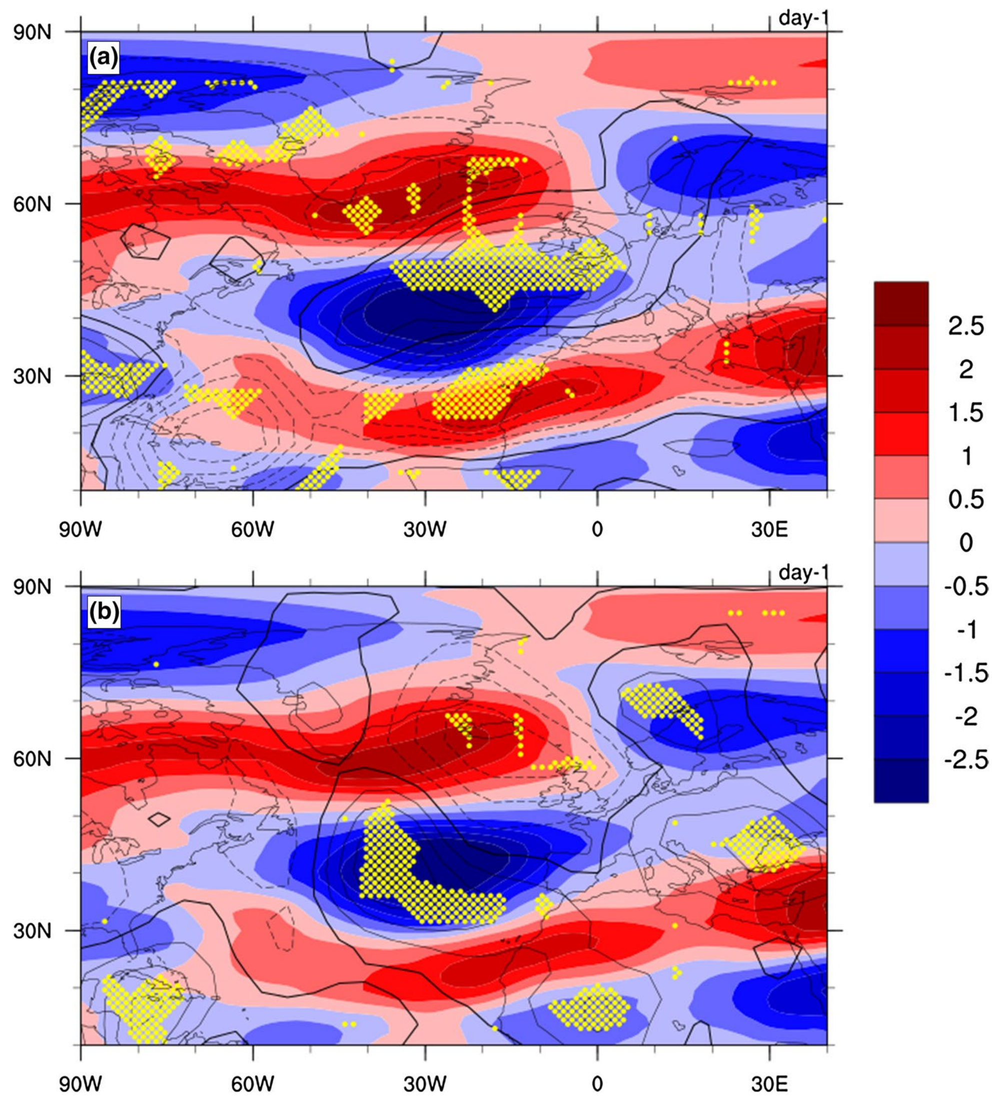

Fig. 13 Differences between HRES and SMTH in **a** anticyclonic and **b** cyclonic Rossby wave breaking frequency (*black contours*, contour interval is 4×10^{-3} day^{-1}, negative values are *dashed*, *thick line* is for the 0 isoline). *Shading* represents zonal wind difference between HRES and SMTH (in m s^{-1}) averaged between 200 and 300 hPa. These results are SMTH experiment in extended winter (Nov–Mar). *Stippling* indicates significant difference in Rossby wave breaking frequency at the 10 % significance level

They are larger over the warm side of the front and mainly originate from wind and stability changes through significant difference of the latent heat flux transfer coefficient. The local hydrostatic pressure adjustment in the MABL is the main mechanism responsible for the surface wind convergence response in the model to the small-scale SST forcing, as suggested by previous studies with similar modeling framework in terms of spatial and time scales. This does not mean that this mechanism explains the full wind response as shown by Takatama et al. (2015). They demonstrate that the downward mixing mechanism explains the wind curl response in their regional model experiments.

The remote influence of small-scale SST patterns has also been investigated. The Atlantic storm track is very sensitive to the presence of small-scale SST patterns in the Gulf Stream region. The latter leads to a southward shift of the storm track density off the coast of North America onto the maximum SST gradient. A significant increase is also depicted over Greenland, the Nordic seas and over the northern part of the Mediterranean basin. Changes are about 10–20 % in these specific regions and involve both storm genesis changes and a shift of the main storm track. Decrease in storm track activity off the North American east coast occurs primarily under BL and AR regimes, while an increase along the warm side of the Gulf Stream SST front and the Mediterranean basin occurs under the EAP and ZO regimes. In summary, it seems that the main mean effect of the small-scale SST patterns is to lead to a more zonally-oriented storm track with a slight southward shift off the North American east coast. Changes also occur with regard to the upper tropospheric zonal wind. The effect of small-scale SST patterns manifests as a tripolar structure of zonal winds with an increase south of Greenland, a decrease in the central North Atlantic and a slight northward shift of the subtropical jet. These changes have been linked to changes in spatial patterns of anticyclonic and cyclonic RWB frequency. Cyclonic RWB changes seem to be the main driver of the acceleration and shift of the subtropical jet over the eastern Mediterranean region. Note also that the increase of cyclonic RWB south of Greenland could explain the slight reduction in BL occurrence frequency, as suggested by Michel and Rivière (2011). The RWB changes thus would support the prominent role of RWB in shaping the upper-tropospheric zonal wind response to the presence of small-scale SST patterns.

Future work will address the same questions in a fully coupled framework using partial coupling experiments and switching on and off the spatial smoothing of the SST coupling field in the region where coupling is active. The sensitivity of the atmospheric response to small-scale SST patterns should be investigated by using different surface flux and MABL parameterizations. This could also help explaining the underestimation of air–sea interaction during summer. These model sensitivity studies should be done in both forced and coupled mode. Other regions where the small-scale air–sea interaction is strong, such as the Kuroshio and the Southern Ocean, should be investigated as well.

Acknowledgments We thank Fabrice Chauvin and Gwendal Rivière for their assistance in the use of the cyclone detection and Rossby wave breaking algorithms as well as Christophe Cassou for useful discussions. Marie Piazza is supported through a joint EDF-CNRS doctoral fellowship and the ASIV project funded by the French National Research Agency under Contract No. ANR 2011 Blanc SIMI 5-6 01403. Some analyses and graphics have been done using the NCAR Command Language (NCL 2013).

References

Ayrault F, Joly A (2000) The genesis of mid-latitude cyclones over the Atlantic ocean: a new climatological perspective. C R Acad Sci Paris Earth Planet Sci 330:173–178. doi:10.1016/S1251-8050(00)00121-X

Booth JF, Thompson L, Patoux J, Kelly KA (2012) Sensitivity of midlatitude storm intensification to perturbations in the sea surface temperature near the Gulf Stream. Mon Weather Rev 140:1241–1256

Bougeault P (1985) A simple parameterization of the large-scale effects of cumulus convection. Mon Weather Rev 113(12):2108–2121. doi:10.1175/1520-0493(1985)113<2108:ASPOTL>2.0.CO;2

Brachet S, Codron F, Feliks Y, Ghil M, Le Treut H, Simonnet E (2012) Atmospheric circulations induced by a midlatitude SST front: a GCM study. J Clim 25(6):1847–1853

Brachet S, Codron F, Feliks Y, Ghil M, Le Treut H, Simonnet E (2012) Atmospheric circulations induced by a midlatitude SST front: a GCM study. J Clim 25(6):1847–1853

Brayshaw DJ, Hoskins B, Blackburn M (2008) The storm-track response to idealized SST perturbations in an aquaplanet GCM. J Atmos Sci 65(9):2842–2860

Bryan FO, Tomas R, Dennis JM, Chelton DB, Loeb NG, McClean JL (2010) Frontal scale air–sea interaction in high-resolution coupled climate models. J Clim 23:6277–6291. doi:10.1175/2010JCLI3665.1

Chelton DB, Xie S-P (2010) Coupled ocean–atmosphere interaction at oceanic mesoscales. Oceanography 23:52–69

Dee DP et al (2011) The ERA-interim reanalysis: configuration and performance of the data assimilation system. Q J R Meteorol Soc 137(656):553–597

Dunbar RS, Lungu T, Weiss B, Stiles B, Huddleston J, Callahan PS, Shirtliffe G, Perry KL, Hsu C, Mears C, Wentz F, Smith D (2006) QuikSCAT science data product user manual, version 3.0, JPL Document D-18053—Rev A, Jet Propulsion Laboratory, Pasadena, CA

Feliks Y, Ghil M, Simonnet E (2004) Low-frequency variability in the midlatitude atmosphere induced by an oceanic thermal front. J Atmos Sci 61:961

Feliks Y, Ghil M, Simonnet E (2007) Low-frequency variability in the midlatitude baroclinic atmosphere induced by an oceanic thermal front. J Atmos Sci 64:97–116

Giordani H, Caniaux G (2001) Sensitivity of cyclogenesis to sea surface temperature in the northwestern Atlantic. Mon Weather Rev 129(6):1273–1295

Hannachi A, Barnes EA, Woollings T (2013) Behaviour of the winter North Atlantic eddy-driven jet stream in the CMIP3 integrations. Clim Dyn 41(3–4):995–1007

Hoskins BJ, Valdes PJ (1990) On the existence of storm-tracks. J Atmos Sci 47:1854–1864

Kilpatrick T, Schneider N, Qiu B (2014) Boundary layer convergence induced by strong winds across a midlatitude SST front. J Clim 27(4):1698–1718. doi:10.1175/JCLI-D-13-00101.1

Kushnir Y, Robinson WA, Bladé I, Hall NMJ, Peng S, Sutton R (2002) Atmospheric GCM response to extratropical SST anomalies: synthesis and evaluation. J Clim 15:2233–2256

Kuwano-Yoshida A, Minobe S, Xie S-P (2010) Precipitation response to the Gulf Stream in an atmospheric GCM. J Clim 23:3676–3698. doi:10.1175/2010jcli3261.1

Laîné A, Lapeyre G, Rivière G (2011) A quasi-geostrophic model for moist storm-tracks. J Atmos Sci 68:1306–1322

Lindzen RS, Nigam S (1987) On the role of sea surface temperature gradients in forcing low-level winds and convergence in the tropics. J Atmos Sci 44(17):2418–2436

Liu J-W, Xie S-P, Norris JR, Zhang S-P (2014) Low-level cloud response to the Gulf Stream front in winter using Calipso. J Clim 27:4421–4432

Louis JF (1979) A parametric model of vertical eddy fluxes in the atmosphere. Bound-Layer Meteorol 17:187–202

Maloney ED, Chelton DB (2006) An assessment of sea surface temperature influence on surface winds in numerical weather prediction and climate models. J Clim 19:2743–2762

Michel C, Rivière G (2011) The link between Rossby wave breakings and weather regime transitions. J Atmos Sci 68:1730–1748

Michel C, Rivière G, Terray L, Joly B (2012) The dynamical link between surface cyclones, upper-tropospheric Rossby wave breaking and the life cycle of the Scandinavian blocking. Geophys Res Lett 39:L10806. doi:10.1029/2012GL051682

Minobe S, Kuwano-Yoshida A, Komori N, Xie S-P, Small RJ (2008) Influence of the Gulf Stream on the troposphere. Nature 452:206–209

Nakamura H, Yamane S (2009) Dominant anomaly patterns in the near-surface baroclinicity and accompanying anomalies in the atmosphere and oceans. Part I: North Atlantic Basin. J Clim 22:880–904. doi:10.1175/2008JCLI2297.1

Nakamura H, Sampe T, Goto A, Ohfuchi W, Xie S-P (2008) On the importance of midlatitude oceanic frontal zones for the mean state and dominant variability in the tropospheric circulation. Geophys Res Lett 35:L15709

NCL (2013) The NCAR command language (version 6.1.2) [software]. UCAR/NCAR/CISL/VETS, Boulder. doi:10.5065/D6WD3XH5

O'Neill LW, Esbensen SK, Thum N, Samelson RM, Chelton DB (2010) Dynamical analysis of the boundary layer and surface wind responses to mesoscale SST perturbations. J Clim 23(3):559–581

Perlin N, De Szoeke SP, Chelton DB, Samelson RS, Skyllingstad ED, O'Neill LarryW (2014) Modeling the atmospheric boundary layer wind response to mesoscale sea surface temperature perturbations. Mon Weather Rev. doi:10.1175/MWR-D-13-00332.1

Putrasahan DA, Miller AJ, Seo H (2013) Isolating mesoscale coupled ocean–atmosphere interactions in the Kuroshio Extension region. Dyn Atmos Oceans 63:60–78. doi:10.1016/j.dynatmoce.2013.04.001

Reynolds RW, Smith TM, Liu C, Chelton DB, Casey KS, Schlax MG (2007) Daily high-resolution-blended analyses for sea surface temperature. J Clim 20(22):5473–5496

Rivière G (2009) Effect of latitudinal variations in low-level baroclinicity on eddy life cycles and upper-tropospheric wave-breaking processes. J Atmos Sci 66:1569–1592

Shimada T, Minobe S (2011) Global analysis of the pressure adjustment mechanism over sea surface temperature fronts using AIRS/Aqua data. Geophys Res Lett 38:L06704. doi:10.1029/2010GLO46625

Small RJ, DeSzoeke SP, Xie SP, O'Neill L, Seo H, Song Q, Cornillon P, Spall M, Minobe S (2008) Air–sea interaction over ocean fronts and eddies. Dyn Atmos Ocean 45:274–319. doi:10.1016/j.dynatmoce.2008.01.001

Small RJ, Tomas RA, Bryan FO (2014) Storm track response to ocean fronts in a global high-resolution climate model. Clim Dyn. doi:10.1007/s00382-013-1980-9

Strong C, Magnusdottir G (2008) Tropospheric Rossby wave breaking and the NAO/NAM. J Atmos Sci 65:2861–2876. doi:10.1175/2008JAS2632.1

Taguchi B, Nakamura H, Nonaka M, Xie S-P (2009) Influences of the Kuroshio/Oyashio extensions on air–sea heat exchanges and storm track activity as revealed in regional atmospheric model simulations for the 2003/04 cold season. J Clim 22:6536–6560

Takatama K, Minobe S, Inatsu M, Small RJ (2012) Diagnostics for near-surface wind convergence/divergence response to the Gulf Stream in a regional atmospheric model. Atmos Sci Lett 1:16–21

Takatama K, Minobe S, Inatsu M, Small RJ (2015) Diagnostics for near-surface wind response to the Gulf Stream in a regional atmospheric model. J Clim 28:238–255. doi:10.1175/JCLI-D-13-00668.1

Vautard R (1990) Multiple weather regimes over the North Atlantic: analysis of precursors and successors. Mon Weather Rev 118(10):2056–2081

Voldoire A et al (2013) The CNRM-CM5.1 global climate model: description and basic evaluation. Clim Dyn 40(9–10):2091–2121

Wallace JM, Mitchell TP, Deser C (1989) The influence of sea-surface temperature on surface wind in the eastern equatorial Pacific: seasonal and interannual variability. J Clim 2(12):1492–1499

Woollings T, Hoskins B, Blackburn M, Hassell D, Hodges K (2010) Storm track sensitivity to sea surface temperature resolution in a regional atmosphere model. Clim Dyn 35:341. doi:10.1007/s00382-009-0554-3